

RECENT UPDATE OF GAS-PHASE CHEMICAL REACTIONS AND MOLECULAR LINES OF TiO IN CLOUDY

Gargi Shaw¹, Gary J. Ferland², Phillip Stancil³, Ryan Porter⁴

RESUMEN

Presentamos nuestra actualización actual sobre las reacciones químicas en fase gaseosa y espectrales líneas de TiO en el código de síntesis espectral CLOUDY. Para ello, hemos añadido 229 reacciones relacionadas con el Ti en la red química. Además, consideramos 230 niveles de energía de estructura fina, los correspondientes 223 transiciones radiativas, y 444 transiciones colisionales con orto y para H₂ y predecir 66 líneas de TiO. Realizamos simulaciones espectroscópicas de la emisión de TiO desde la región circunestelar de la supergigante roja rica en oxígeno VY Canis Majoris para validar nuestra actualización. Nuestro modelo reproduce la densidad de la columna de TiO observada. Esta actualización es útil para modelar entornos astrofísicos libres de polvo donde el Ti está en fase gaseosa y se puede formar TiO.

ABSTRACT

We present our current update on the gas-phase chemical reactions and spectral lines of TiO in the spectral synthesis code CLOUDY. For this purpose, we have added 229 Ti-related reactions in the chemical network. In addition, we consider 230 fine-structure energy levels, the corresponding 223 radiative transitions, and 444 collisional transitions with ortho and para H₂ and predict 66 TiO lines. We perform spectroscopic simulations of TiO emission from the circumstellar region of the oxygen-rich red supergiant VY Canis Majoris to validate our update. Our model reproduces the observed TiO column density.

This update is helpful in modeling dust-free astrophysical environments where Ti is in the gas phase and TiO can form.

Key Words: Astronomy software — Computational methods — Galaxy — Molecular data

1. INTRODUCTION

The spectroscopic simulation code CLOUDY simulates the conditions in a non-equilibrium astrophysical plasma and predicts the resulting spectrum and column densities of various ions, neutrals, and molecules(Chatzikos et al. 2023; Gunasekera et al. 2023; Ferland et al. 2017, 2013). Our aim is to predict more molecular lines with better precision. Hence, we regularly update our chemical network and incorporate improved chemical reactions and internal structures for our existing chemistry whenever new or better data are available

(Shaw et al. 2017, 2020, 2023, 2022) and add new molecules as the astrophysical need arises. One such molecule is TiO, a possible precursor of inorganic dust (Danilovich et al. 2020).

TiO is the dominant source of opacity in the atmosphere of cool stars (Lodders 2002) and is observed in the atmosphere of giant M stars (Jorgensen 1994; Kamiński et al. 2013b). Kamiński et al. (2013a) observed pure rotational lines of TiO in the circumstellar envelope of the red supergiant VY Canis Majoris (VY CMa). The observed column density of TiO in VY CMa is $(6.7 \pm 0.8) \times 10^{15} \text{ cm}^{-2}$. They also observed TiO₂. In an oxygen-rich circumstellar envelope, nearly all carbon is locked into CO, and hence, TiO forms and can act as an important seed for inorganic dust formation (Gail & Sedlmayr 1998). Kamiński et al. (2013b) showed that for VY CMa, the dust and TiO emission come from different regions. Their formation regions are separated

¹Department of Astronomy and Astrophysics, Tata Institute of Fundamental Research, Mumbai 400005, India

²Physics & Astronomy, University of Kentucky, Lexington, Kentucky, USA

³Physics & Astronomy, University of Georgia, Georgia, USA

⁴Stellar Science, 6565 Americas Pkwy 925, Albuquerque, NM 87110, USA

by about $0''.15$ corresponding to 2.7×10^{13} cm assuming the distance of VY CMa is 1.20 kpc (Zhang et al. 2012). This confirms that TiO is present in the dust-free region of VY CMa.

The solar abundance of Ti is 8.91×10^{-8} Grevesse et al. (2010). However, TiO is not observed in the ISM due to the high depletion of Ti (Welsh et al. 1997). In dust-free environments, Ti is in the gas phase and TiO can form.

Here, we aim to include the gas-phase chemical reactions and spectral lines of TiO in the spectral synthesis code Cloudy (Chatzikos et al. 2023; Gunasekera et al. 2023) which will be useful in modeling dust-free astrophysical environments where TiO is in the gas phase. These updates will be part of the upcoming 2024 release of Cloudy.

2. CALCULATIONS AND RESULTS

2.1. Updated Ti-chemistry in CLOUDY

There is a scarcity of reaction rates for Ti-chemistry due to its very low abundance in the ISM. It is not included in the UMIST Database for Astrochemistry (UDfA) (McElroy et al. 2013) or in Kinetic Database for Astrochemistry (KIDA) (Wakelam et al. 2012). We incorporate available reactions(Tsai et al. 2021; Churchwell et al. 1980; Ramírez et al. 2020), but these are small in number.

We adopted Si-based chemistry as a proxy for the missing Ti chemistry. Both Ti and Si are important refractory elements (Gilli et al. 2006). In addition, Ti-oxides and Si-oxides are precursors of inorganic dust, and Si-chemistry is well-studied and documented. Hence, for the rest of the Ti-related reactions, we copied analogous reactions involving Si from UDfA. All the reactions in our new network are given in the appendix.

A large number of models covering diverse astrophysical environments are publicly available with the CLOUDY download under the directory `tsuite`. We compare `tsuite` model predictions every day to monitor the changes in species abundances and line intensities as a result of changes in the source code and atomic and molecular data. The Cloudy test suite is extensive and includes simulations at very low and very high temperatures, CMB to 10^{10} K. The chemistry must work for all conditions. Often we encounter problems with the extrapolation of simple fits to the temperature range we need for chemical rate coefficients. To overcome this problem, we apply a temperature cap, T_{cap} , for $\beta > 0$ (See appendix). For $T > T_{cap}$, the rate coefficients retain the same values as at T_{cap} . Though ad-hoc, we choose $T_{cap}=2500$ K (Shaw et al. 2023). The chemical network is very sensitive to small changes in rate

coefficients. Hence, for any chemical update to pass through all the `tsuite` models simultaneously is hard and time-consuming. We critically examine each update if it results in a relative change of greater than $\pm 30\%$ in column density or line intensity.

In this work, some updates produce a relative change of greater than $\pm 90\%$ in column density.

We find that the two reactions, $H_3O^+ + SiO \rightarrow SiOH^+ + H_2O$ and $H_3+ SiO \rightarrow SiOH^+ + H_2$, produced significant changes in $SiOH^+$ column densities with the updated UDfA2012 rate coefficients. The UDfA2012 rate coefficients for the reactions, $HSiO_2^+ + e \rightarrow SiO_2 + H$ and $OH + SiO \rightarrow SiO_2 + H$ result in convergence problem for high density ($> 10^{17} \text{ cm}^{-3}$) and low radiation model. Hence, we retain the UDfA2006 rate coefficients for these two reactions.

We calculate the line luminosities/intensities from energy levels and radiative and collisional rate coefficients in the Leiden Atomic and Molecular Database (LAMDA) format (Schöier et al. 2005). TiO energy levels and radiative rate coefficients are from the Cologne Database for Molecular Spectroscopy (CDMS) (<https://cdms.astro.uni-koeln.de/>). The ground state of TiO is triplet-delta with lambda splitting. We consider 230 energy levels, and the corresponding 223 radiative transitions. In addition, we consider 444 collisional transitions with ortho and para H_2 . The collisional transitions of CO with ortho and para H_2 are modified from Yang et al. (2010) as a proxy for ortho and para H_2 collisions with TiO. In cases for $J_{low}=3$ there are four possible transitions, so the CO rates were divided by 4. For $J_{low}=2$ and $J_{low}=1$, CO rates were divided by 3 and 2, respectively. Otherwise, each CO rate was divided by 5. The temperature range for collisional rates vary from 2 to 3000 K. These were compiled and converted to LAMDA format. This will be part of upcoming 2024 release of Cloudy. In the future, we will replace these collisional rates with actual data when they become available. We will also add collisional rate coefficients for other colliders, H and He, when data becomes available.

2.2. Modelling TiO from VY Canis Majoris

We present a model for the circumstellar envelope of the red supergiant VY CMa to validate our Ti-chemical network. All calculations are done using the development version of Cloudy (Chatzikos et al. 2023; Gunasekera et al. 2023). VY CMa has a rich inventory of various molecules (Kamiński et al. 2013b). However, here we concentrate mainly on TiO.

We consider a spherical model with the ionizing source, star, at the centre. Cloudy requires basic

input parameters such as the radiation field, density at the inner radius which is illuminated by the starlight, chemical abundances, etc. Observations reveal the effective temperature of the central star is 3650 K (Massey et al. 2006) with a luminosity of $(3 \pm 0.5) \times 10^5 L_\odot$ (Choi et al. 2008). We use this observed value to set the SED of the radiation field.

VY CMa is a large star with $R_\star = 1420 \pm 120 R_\odot$ (Wittkowski et al. 2012). We consider the inner radius of the circumstellar envelope to be at R_\star . TiO is expected to form nearer the star, where the temperature is high, above the sublimation temperature of dust. Decin et al. (2016) have observed that NaCl forms at $R < 250 R_\star$ from the central star. Kamiński et al. (2013a) also noticed that the main component of the TiO emission covers the same velocity range as the NaCl profile, but is confined within $R = 28 \times R_\star$. The Dissociation energy of TiO is much higher than NaCl, so in the gas phase it is expected to peak closer to the central star than NaCl. Since our main focus is TiO, we further confine our model to $R = 28 \times R_\star$ from the central star.

For an oxygen-rich environment, nearly all carbon is locked up in CO. Thus, formation of silicate dusts is more favourable than the formation of graphite dust, when physical conditions permit. The sublimation temperature of silicate dusts is ≈ 1400 K. Furthermore, Kamiński et al. (2013a) estimated $T_{rot} = 1010 \pm 870$ K. So, we further constrain our model to have a temperature above > 1400 K.

The density, in general, depends on the distance from the central source of ionization. We consider the density to be proportional to r^{-2} , consistent with a $v \propto r$ wind (Keady et al. 1988; Ziurys 2006). In addition, it is known that the density of the circumstellar envelope can vary over a wide range. Hence, in our grid models, we vary the density $n_H(r_{in})$ (the density at the inner radius (r_{in}) of the circumstellar envelope) from 10^9 to $10^{12.5} \text{ cm}^{-3}$ in steps of 0.25 dex. We consider solar abundances of elements as reported in Grevesse et al. (2010), and we do not include dust in our model. Finally, we include a background cosmic ray ionization rate (important for the ion balance in molecular regions) of $2 \times 10^{-16} \text{ s}^{-1} \text{ s}^{-1}$ in our grid models (Shaw et al. 2008; Shaw & Ferland 2021).

Figure 1 shows our model's predicted TiO column density as a function of hydrogen number density, $n_H(r_{in})$. The solid horizontal lines represent the observed column density range Kamiński et al. (2013a). From the plot, we conclude that the observed TiO column density comes from a region with

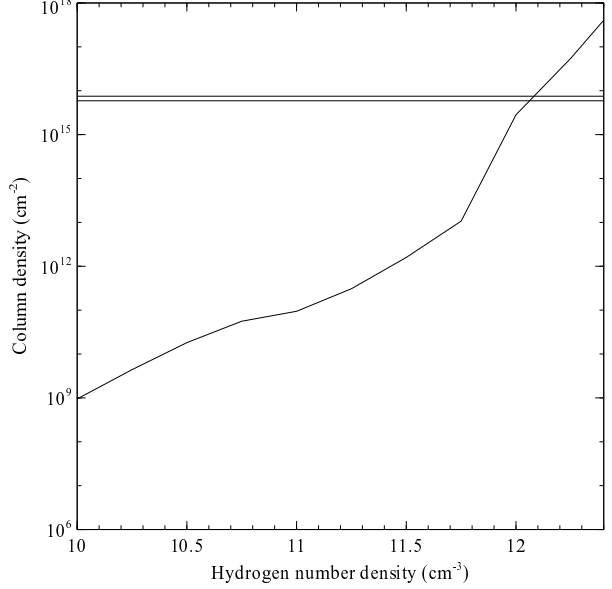


Fig. 1. Column density of TiO as a function of $n_H(r_{in})$. The horizontal lines represent the observed column density range.

$$n_H(r_{in}) = 10^{12.06} \text{ to } 10^{12.08} \text{ cm}^{-3}.$$

Next, we consider a single model with $n_H(r_{in}) = 10^{12.07} \text{ cm}^{-3}$, holding other parameters constant. Figure 2 shows the variation of TiO, TiO^+ , TiO_2 , Ti, Ti^+ as a function of the depth of the cloud from the illuminated surface. The temperature varies from 3431 K to 1400 K across the region considered. We find that Ti is mostly ionic, and the dominant oxide form of Ti is TiO.

Our model's predicted neutral hydrogen column density is $\approx 8 \times 10^{25} \text{ cm}^{-2}$. Although our model does not include dust, it predicts a high H_2 column density $\approx 10^{18} \text{ cm}^{-2}$. This is due to the presence of a significant H^- abundance which helps to form H_2 in dust-free environments (Shaw et al. 2005). However, this single model predicts a TiO_2 column density, $7.16 \times 10^{12} \text{ cm}^{-2}$, much below the observed value.

Figure 3 shows the line intensity of TiO lines for this single model assuming the distance of VY CMa is 1.20 kpc (Zhang et al. 2012).

Earlier, (Gail & Sedlmayr 1998) have showed that TiO_2 forms at a much lower temperature than TiO. So, we recomputed the same single model but removing the 1400 K temperature limit. The predicted TiO and TiO_2 column densities are 7.5×10^{15} and $8.7 \times 10^{15} \text{ cm}^{-2}$, respectively. The observed TiO_2 column density is $(5.65 \pm 1.33) \times 10^{15} \text{ cm}^{-2}$ (De Beck et al. 2015). Both of these molecules are confined within $R = 28 \times R_\star$. The corresponding ionization structure is shown in Figure 4. We no-

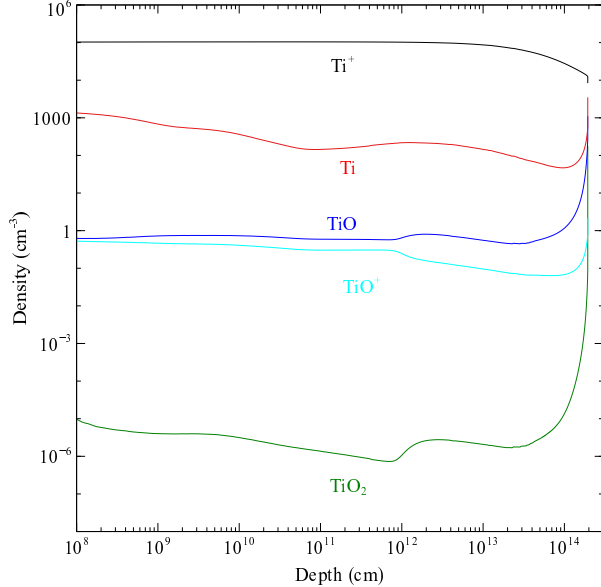


Fig. 2. Variation of TiO , TiO^+ , TiO_2 , Ti , Ti^+ as a function of cloud depth. The gas temperature is > 1400 K.

nice that as the temperature decreases below 1400 K, more TiO_2 is formed. We conclude that Ti is locked in TiO above 1400 K and in TiO_2 at a lower temperature. Since silicate dust can form below 1400K, we conclude that TiO_2 remains in the gas phase outside the dust-formation zone, and might play only a minor role in the dust-condensation process around VY CMa. The same conclusion was made by De Beck et al. (2015).

2.3. Effects of input parameters

There is a debate regarding the luminosity and radius of the star VY CMa. Massey et al. (2006) have estimated the luminosity and radius to be $6 \times 10^4 \text{ L}_\odot$ and 600 R_\odot , respectively. However, Wittkowski et al. (2012) have estimated these to be $5 \times 10^5 \text{ L}_\odot$ and $R_\star = 1420 \pm 120 \text{ R}_\odot$, respectively. Here, we show the effects of various input parameters on the predicted hydrogen number density, column densities of TiO and TiO_2 for the above-mentioned model of VY CMa.

Firstly, we consider a value, $1.0 \times 10^5 \text{ L}_\odot$, instead of $2.5 \times 10^5 \text{ L}_\odot$ considered in section 2.2. We run a similar grid of models varying $n_H(r_{in})$ from 10^9 to $10^{12.5} \text{ cm}^{-3}$ in steps of 0.25 dex, keeping all the other parameters the same. For this case, the observed TiO column density comes from a region with $n_H(r_{in}) = 10^{11.79}$ to $10^{11.80} \text{ cm}^{-3}$. This is lower by ≈ 0.3 dex from the value derived in section 2.2.

Next, we consider a lower value of $R_\star = 770 \text{ R}_\odot$

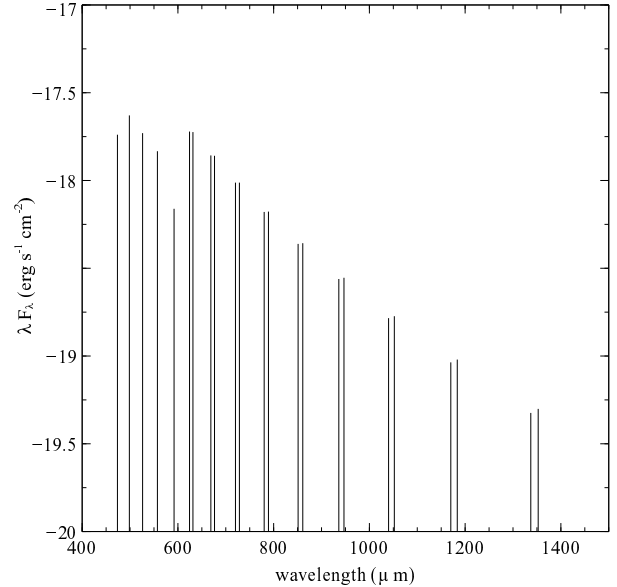


Fig. 3. Intensity of TiO lines

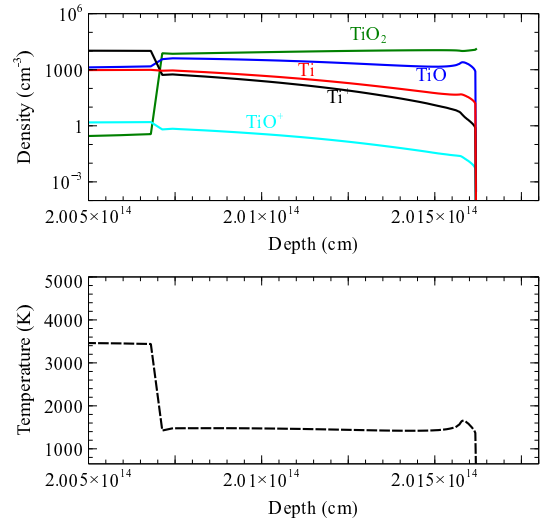


Fig. 4. Variation of TiO , TiO^+ , TiO_2 , Ti , Ti^+ , and temperature as a function of cloud depth.

compared to the earlier value of $R_\star=1540 \text{ R}_\odot$ for VY CMa, and run a similar grid model keeping other parameters fixed. For this case, the observed TiO column density comes from a region with $n_H(r_{in}) = 10^{12.66}$ to $10^{12.67} \text{ cm}^{-3}$. This is higher by ≈ 0.6 dex from the value derived in section 2.2.

Further, we change the density to be proportional to r^{-3} , and run a similar grid model keeping other parameters fixed as described in section 2.2. We find

that with the new density law, the observed TiO column density comes from a region with $n_H(r_{in}) = 10^{12.28}$ to $10^{12.31} \text{ cm}^{-3}$. This is higher by ≈ 0.2 dex from the value derived in section 2.2.

We notice that the value of $n_H(r_{in})$ is more dependent on the inner radius r_{in} of the envelope. However, for all these cases, as the temperature decreases below 1400 K, more TiO_2 is formed. Similarly, both TiO and TiO_2 are confined within $R = 28 \times R_\star$.

2.4. Model limitations

Like every astrophysical model, our model also has some limitations. The main limitations are listed below.

Firstly, most of our Ti-related gas-phase chemical reaction rate coefficients involving Ti are copied from analogous Si-related reactions. Secondly, we have considered only ortho and para- H_2 collisional excitation and deexcitation. Thirdly, we have assumed a spherical geometry. However, observations suggest that the geometry is not perfectly spherical. Despite these limitations, our model predicts the observed column density of TiO and TiO_2 .

3. DISCUSSIONS AND CONCLUSIONS

In this work, we updated gas-phase chemical reaction rates and molecular lines arising from TiO in the spectral synthesis code CLOUDY. We have added 229 reactions in the chemical network. In addition, we consider 230 energy levels, corresponding radiative transitions, and 444 collisional transitions with ortho and para H_2 . These molecular lines can be observed using ALMA and JWST. These updates will be part of the upcoming 2024 release of Cloudy.

Our main conclusions from this work are:

1. In the gas-phase, Ti is mainly in TiO for temperatures above 1400 K. Whereas, TiO_2 dominates at a lower temperature.
2. Our model predicts the observed column densities of TiO and TiO_2 around the oxygen rich red super giant VY CMa. Both of these molecules are confined within $R = 28 \times R_\star$. However, TiO forms closer to the central star when temperatures are above 1400K.
3. Few ISM-appropriate Ti molecular reaction networks exist due to its low gas-phase abundance in the ISM. Most of our Ti-related gas-phase chemical reaction rate-coefficients are copied from analogous Si-related reactions. Our model does predict observed TiO and TiO_2 column

density around VY CMa. However, we look forward to actual rate coefficients for these reactions.

In future, we hope to incorporate another important precursor of inorganic dust, AlO, into CLOUDY's chemical network.

4. ACKNOWLEDGMENTS

We thank Peter van-hoof, Kyle Walker, and Krishal Patel for their valuable help. GS acknowledges support from DST/WOS-A/PM-2/2021.

REFERENCES

- Chatzikos, M., Bianchi, S., Camilloni, F., Chakraborty, P., Gunasekera, C. M., Guzmán, F., Milby, J. S., Sarkar, A., Shaw, G., van Hoof, P. A. M., & Ferland, G. J. 2023, RMxAA, 59, 327
 Choi, Y. K., Hirota, T., Honma, M., Kobayashi, H., Bushimata, T., Imai, H., Iwadate, K., Jike, T., Kameno, S., Kameya, O., Kamohara, R., Kan-Ya, Y., Kawaguchi, N., Kijima, M., Kim, M. K., Kuji, S., Kurayama, T., Manabe, S., Maruyama, K., Matsui, M., Matsumoto, N., Miyaji, T., Nagayama, T., Nakagawa, A., Nakamura, K., Oh, C. S., Omodaka, T., Oyama, T., Sakai, S., Sasao, T., Sato, K., Sato, M., Shibata, K. M., Tamura, Y., Tsushima, M., & Yamashita, K. 2008, PASJ, 60, 1007
 Churchwell, E., Hocking, W. H., Merer, A. J., & Gerry, M. C. L. 1980, AJ, 85, 1382
 Dalgarno, A. & McCray, R. A. 1973, ApJ, 181, 95
 Danilovich, T., Gottlieb, C. A., Decin, L., Richards, A. M. S., Lee, K. L. K., Kamiński, T., Patel, N. A., Young, K. H., & Menten, K. M. 2020, ApJ, 904, 110
 De Beck, E., Vlemmings, W., Muller, S., Black, J. H., O'Gorman, E., Richards, A. M. S., Baudry, A., Maercker, M., Decin, L., & Humphreys, E. M. 2015, A&A, 580, A36
 Decin, L., Richards, A. M. S., Millar, T. J., Baudry, A., De Beck, E., Homan, W., Smith, N., Van de Sande, M., & Walsh, C. 2016, A&A, 592, A76
 Ferland, G. J., Chatzikos, M., Guzmán, F., Lykins, M. L., van Hoof, P. A. M., Williams, R. J. R., Abel, N. P., Badnell, N. R., Keenan, F. P., Porter, R. L., & Stancil, P. C. 2017, RMxAA, 53, 385
 Ferland, G. J., Porter, R. L., van Hoof, P. A. M., Williams, R. J. R., Abel, N. P., Lykins, M. L., Shaw, G., Henney, W. J., & Stancil, P. C. 2013, RMxAA, 49, 137
 Gail, H. P. & Sedlmayr, E. 1998, Faraday Discussions, 109, 303
 Gilli, G., Israelian, G., Ecuvillon, A., Santos, N. C., & Mayor, M. 2006, A&A, 449, 723
 Grevesse, N., Asplund, M., Sauval, A. J., & Scott, P. 2010, Ap&SS, 328, 179
 Gunasekera, C. M., van Hoof, P. A. M., Chatzikos, M., & Ferland, G. J. 2023, Research Notes of the American Astronomical Society, 7, 246

- Indriolo, N., Geballe, T. R., Oka, T., & McCall, B. J. 2007, *ApJ*, 671, 1736
- Jørgensen, U. G. 1994, *A&A*, 284, 179
- Kamiński, T., Gottlieb, C. A., Menten, K. M., Patel, N. A., Young, K. H., Brünken, S., Müller, H. S. P., McCarthy, M. C., Winters, J. M., & Decin, L. 2013a, *A&A*, 551, A113
- Kamiński, T., Gottlieb, C. A., Young, K. H., Menten, K. M., & Patel, N. A. 2013b, *ApJS*, 209, 38
- Keady, J. J., Hall, D. N. B., & Ridgway, S. T. 1988, *ApJ*, 326, 832
- Lodders, K. 2002, *The Astrophysical Journal*, 577, 974 [LINK]
- Massey, P., Levesque, E. M., & Plez, B. 2006, *ApJ*, 646, 1203
- McElroy, D., Walsh, C., Markwick, A. J., Cordiner, M. A., Smith, K., & Millar, T. J. 2013, *A&A*, 550, A36
- Ramírez, V., Cridland, A. J., & Mollière, P. 2020, *A&A*, 641, A87
- Schöier, F. L., van der Tak, F. F. S., van Dishoeck, E. F., & Black, J. H. 2005, *A&A*, 432, 369
- Shaw, G., Ferland, G., & Chatzikos, M. 2023, *Research Notes of the American Astronomical Society*, 7, 45
- Shaw, G., Ferland, G., & Chatzikos, M. 2023, *Research Notes of the AAS*, 7, 153 [LINK]
- Shaw, G. & Ferland, G. J. 2021, *ApJ*, 908, 138
- Shaw, G., Ferland, G. J., Abel, N. P., Stancil, P. C., & van Hoof, P. A. M. 2005, *ApJ*, 624, 794
- Shaw, G., Ferland, G. J., & Chatzikos, M. 2022, *ApJ*, 934, 53
- Shaw, G., Ferland, G. J., & Hubeny, I. 2017, *ApJ*, 843, 149
- Shaw, G., Ferland, G. J., & Ploeckinger, S. 2020, *Research Notes of the American Astronomical Society*, 4, 78
- Shaw, G., Ferland, G. J., Srianand, R., Abel, N. P., van Hoof, P. A. M., & Stancil, P. C. 2008, *ApJ*, 675, 405
- Tsai, S.-M., Malik, M., Kitzmann, D., Lyons, J. R., Fa-teev, A., Lee, E., & Heng, K. 2021, *ApJ*, 923, 264
- Wakelam, V., Herbst, E., Loison, J. C., Smith, I. W. M., Chandrasekaran, V., Pavone, B., Adams, N. G., Bacchus-Montabonel, M. C., Bergeat, A., Béroff, K., Bierbaum, V. M., Chabot, M., Dalgarno, A., van Dishoeck, E. F., Faure, A., Geppert, W. D., Gerlich, D., Galli, D., Hébrard, E., Hersant, F., Hickson, K. M., Honvault, P., Klippenstein, S. J., Le Picard, S., Nyman, G., Pernot, P., Schlemmer, S., Selsis, F., Sims, I. R., Talbi, D., Tennyson, J., Troe, J., Wester, R., & Wiesenfeld, L. 2012, *ApJS*, 199, 21
- Welsh, B. Y., Sasseen, T., Craig, N., Jelinsky, S., & Albert, C. E. 1997, *ApJS*, 112, 507
- Wittkowski, M., Hauschildt, P. H., Arroyo-Torres, B., & Marcaide, J. M. 2012, *A&A*, 540, L12
- Yang, B., Stancil, P. C., Balakrishnan, N., & Forrey, R. C. 2010, *ApJ*, 718, 1062
- Zhang, B., Reid, M. J., Menten, K. M., & Zheng, X. W. 2012, *ApJ*, 744, 23
- Ziurys, L. M. 2006, *Proceedings of the National Academy of Science*, 103, 12274

G. Shaw, Department of Astronomy and Astrophysics, Tata Institute of Fundamental Research, Mumbai 400005, India (gargishaw@gmail.com).
 G. Ferland, Physics & Astronomy, University of Kentucky, Lexington KY 40506, USA (gary@uky.edu).
 P. Stancil, Department of Physics and Astronomy and Center for Simulational Physics, University of Georgia, USA.
 R. Porter, Stellar Science, 6565 Americas Pkwy 925, Albuquerque, NM 87110, USA

5. APPENDIX

Here we list the rate coefficients used for various Ti-related reactions in Table 1. Ti-related reactions are mainly copied from the analogous Si-related reactions from UDfA2006 and UDfA2012. For example, in the reference column Si5209 refers a copied reaction from Si reaction of UDfA2012 with the reaction number 5209. Ref 1, 2, and 3 refer to Churchwell et al. (1980), Ramírez et al. (2020), and Tsai et al. (2021), respectively. The rate coefficient for the reaction, $\text{Ti}^+ + \text{H}^- \rightarrow \text{Ti} + \text{H}$, is taken from Dalgarno & McCray (1973).

The format for the two-body rate coefficients are given in an Arrhenius-type equation,

$$k = \alpha \left(\frac{T}{300} \right)^\beta \exp(-\gamma/T). \quad (1)$$

where T is the temperature of the gas. Whereas the photoreaction rate coefficients are given by

$$k = \alpha \exp(-\gamma A_V). \quad (2)$$

where A_V is the extinction at visible wavelengths. Details can be found in McElroy et al. (2013). For the two-body reactions and photoreactions, γ depends on the activation energy of the reaction and the increased dust extinction at ultraviolet wavelengths, respectively. It is to be noted, we do not use UDfA cosmic ray ionization rates. Our cosmic-ray ionization rates are normalised to a total rate for electron production from cosmic-ray ionization. We adopt a mean cosmic-ray ionization rate of $2 \times 10^{-16} \text{ s}^{-1}$ for atomic hydrogen as the default background value (Indriolo et al. 2007; Shaw et al. 2008). Shaw & Ferland (2021) showed that this rate is dependent of the presence of PAHs as well. For detail, see Shaw et al. (2022).

TABLE 1: List of Ti related chemical reactions

Begin of Table				
Reactions	α	β	γ	Ref
C + TiH \rightarrow TiC + H	6.59e-11	0	0	Si5209
C + TiH ₂ \rightarrow HCTi + H	1.e-10	0	0	Si5207
N + TiH \rightarrow TiN + H	1.66e-10	-0.09	0	Si5513
N + TiH ₂ \rightarrow HNTi + H	8.0e-11	0.17	0	Si5511
N + TiC \rightarrow Ti + CN	5.0e-11	0	0	Si5509
N + TiC \rightarrow TiN + C	5.e-11	0	0	Si5510
CH ₂ + Ti \rightarrow HCTi + H	1.e-10	0	0	Si5241
O + TiH \rightarrow TiO + H	1.e-10	0	0	Si5665
O + TiH ₂ \rightarrow TiO + H ₂	8.e-11	0	0	Si5661
O + TiH ₂ \rightarrow TiO + H + H	1.2e-10	0	0	Si5662
O + TiC \rightarrow TiO + C	5.e-11	0	0	Si5660
O + TiC \rightarrow Ti + CO	5.e-11	0	0	Si5659
O + HCTi \rightarrow TiO + CH	2.e-11	0	0	Si5626
O + TiN \rightarrow NO + Ti	5.e-11	0	0	Si5666
O + TiN \rightarrow TiO + N	5.75e-11	0.1	200	Si5667
O + TiNC \rightarrow TiN + CO	1.e-11	0	0	Si5668
O + TiC ₂ \rightarrow TiC + CO	4.e-11	0	0	Si5656
OH + Ti \rightarrow TiO + H	1.e-10	0	0	Si5698
OH + TiO \rightarrow TiO ₂ + H	2.e-12	0	0	Si5699
C ₂ H ₂ + Ti \rightarrow TiC ₂ + H ₂	1.30e-10	-0.71	29	Si5100
Ti + O ₂ \rightarrow TiO + O	1.72e-10	-0.53	17	Si5710
H ⁺ + TiH \rightarrow Ti ⁺ + H ₂	1.70e-9	0	0	Si2586
H + TiH ⁺ \rightarrow Ti ⁺ + H ₂	1.9e-9	0	0	Si3069
H ⁺ + TiH ₂ \rightarrow TiH ⁺ + H ₂	1.5e-9	0	0	Si2583
H ⁺ + HCTi \rightarrow TiC ⁺ + H ₂	1.5e-9	0	0	Si2568
H ⁺ + HNTi \rightarrow TiN ⁺ + H ₂	1.5e-9	0	0	Si2571
H + TiS ⁺ \rightarrow HS + Ti ⁺	1.90e-9	0	0	Si3070
H ₂ + TiC ⁺ \rightarrow HCTi ⁺ + H	1.5e-9	0	0	Si2693
H ₂ + TiO ⁺ \rightarrow TiOH ⁺ + H	3.2e-10	0	0	Si2696
H ₃ ⁺ + Ti \rightarrow TiH ⁺ + H ₂	3.7e-9	0	0	Si2964
H ₃ ⁺ + TiH \rightarrow TiH ₂ ⁺ + H ₂	2.e-9	0	0	Si2977
H ₃ ⁺ + TiC \rightarrow HCTi ⁺ + H ₂	3.e-9	0	0	Si2971
H ₃ ⁺ + TiN \rightarrow HNTi ⁺ + H ₂	2.e-9	0	0	Si2978
H ₃ ⁺ + TiO \rightarrow TiOH ⁺ + H ₂	2.e-9	0	0	S2981
H ₃ ⁺ + TiS \rightarrow HTiS ⁺ + H ₂	8.7e-9	-0.5	0	Si2982
He ⁺ + TiH \rightarrow Ti ⁺ + He + H	1.80e-9	0	0	Si3549
He ⁺ + TiH ₂ \rightarrow Ti ⁺ + He + H ₂	1.e-9	0	0	Si3543
He ⁺ + TiH ₂ \rightarrow TiH ⁺ + He + H	1.e-9	0	0	Si3544
He ⁺ + TiC \rightarrow TiC ⁺ + He	2.e-9	-0.5	0	Si3538
He ⁺ + TiC \rightarrow Ti ⁺ + C + He	2.e-9	-0.5	0	Si3537
He ⁺ + HCTi \rightarrow Ti ⁺ + CH + He	1.e-9	0	0	Si3478
He ⁺ + HCTi \rightarrow TiC ⁺ + He + H	1.e-9	0	0	Si3479

Continuation of Table 1				
Reactions	α	β	γ	Ref
$\text{He}^+ + \text{TiN} \rightarrow \text{Ti}^+ + \text{N} + \text{He}$	2.e-9	-0.5	0	Si3550
$\text{He}^+ + \text{HNTi} \rightarrow \text{TiN}^+ + \text{He} + \text{H}$	2.e-9	0	0	Si3488
$\text{He}^+ + \text{TiO} \rightarrow \text{Ti}^+ + \text{O} + \text{He}$	1.e-9	0	0	1
$\text{He}^+ + \text{TiO} \rightarrow \text{Ti} + \text{O}^+ + \text{He}$	8.6e-10	-0.5	0	Si3554
$\text{He}^+ + \text{TiC}_2 \rightarrow \text{Ti}^+ + \text{C}_2 + \text{He}$	2.e-9	-0.5	0	Si3528
$\text{He}^+ + \text{TiNC} \rightarrow \text{Ti} + \text{CN}^+ + \text{He}$	2.e-9	-0.5	0	Si3551
$\text{He}^+ + \text{TiO}_2 \rightarrow \text{O}_2 + \text{Ti}^+ + \text{He}$	2.e-9	0	0	Si3552
$\text{He}^+ + \text{TiS} \rightarrow \text{S} + \text{Ti}^+ + \text{He}$	3.8e-9	-0.5	0	Si3556
$\text{He}^+ + \text{TiS} \rightarrow \text{S}^+ + \text{Ti} + \text{He}$	3.8e-9	-0.5	0	Si13555
$\text{C}^+ + \text{TiH} \rightarrow \text{TiC}^+ + \text{H}$	1.1e-9	0	0	Si1666
$\text{C} + \text{TiH}^+ \rightarrow \text{TiC}^+ + \text{H}$	2.e-10	0	0	Si2146
$\text{C}^+ + \text{TiH}_2 \rightarrow \text{TiC}^+ + \text{H}_2$	1.e-9	0	0	Si1661
$\text{C}^+ + \text{TiH}_2 \rightarrow \text{HCTi}^+ + \text{H}$	1.e-9	0	0	Si1660
$\text{C} + \text{TiH}_2^+ \rightarrow \text{HCTi}^+ + \text{H}$	1.1e-9	0	0	Si2147
$\text{C}^+ + \text{TiC} \rightarrow \text{Ti}^+ + \text{C}_2$	2.50e-9	-0.5	0	Si1655
$\text{C}^+ + \text{HCTi} \rightarrow \text{TiC}_2^+ + \text{H}$	2.e-9	0	0	Si1631
$\text{C}^+ + \text{TiN} \rightarrow \text{TiC}^+ + \text{N}$	1.e-9	-0.5	0	Si1667
$\text{C}^+ + \text{HNTi} \rightarrow \text{TiNC}^+ + \text{H}$	2.e-9	0	0	Si1635
$\text{C}^+ + \text{TiO} \rightarrow \text{Ti}^+ + \text{CO}$	1.e-9	0	0	1
$\text{C} + \text{TiO}^+ \rightarrow \text{Ti}^+ + \text{CO}$	1.e-9	0	0	Si2153
$\text{C}^+ + \text{TiS} \rightarrow \text{TiC}^+ + \text{S}$	2.3e-9	-0.5	0	Si1669
$\text{CH} + \text{Ti}^+ \rightarrow \text{TiC}^+ + \text{H}$	6.3e-10	-0.5	0	Si2487
$\text{CH} + \text{TiH}^+ \rightarrow \text{Ti} + \text{CH}_2^+$	6.e-10	-0.5	0	Si2488
$\text{CH} + \text{TiO}^+ \rightarrow \text{HCO}^+ + \text{Ti}$	5.9e-10	-0.5	0	Si2489
$\text{N} + \text{TiH}^+ \rightarrow \text{TiN}^+ + \text{H}$	2.e-10	0	0	Si3692
$\text{N} + \text{TiH}_2^+ \rightarrow \text{HNTi}^+ + \text{H}$	1.e-10	0	0	Si3693
$\text{N} + \text{TiC}^+ \rightarrow \text{Ti}^+ + \text{CN}$	7.7e-10	0	0	Si3690
$\text{N} + \text{TiO}^+ \rightarrow \text{NO}^+ + \text{Ti}$	9.e-11	0	0	Si3696
$\text{N} + \text{TiO}^+ \rightarrow \text{NO} + \text{Ti}^+$	2.1e-10	0	0	Si3697
$\text{CH}_2 + \text{Ti}^+ \rightarrow \text{HCTi}^+ + \text{H}$	8.7e-10	0	0	Si2239
$\text{CH}_2 + \text{TiO}^+ \rightarrow \text{H}_2\text{CO} + \text{Ti}^+$	7.88e-10	0	0	Si1589
$\text{NH} + \text{Ti}^+ \rightarrow \text{TiN}^+ + \text{H}$	1.e-9	-0.5	0	Si3846
$\text{CH}_3^+ + \text{Ti} \rightarrow \text{HCTi}^+ + \text{H}_2$	2.e-10	0	0	Si2318
$\text{CH}_3 + \text{Ti}^+ \rightarrow \text{HCTi}^+ + \text{H}_2$	1.e-9	0	0	Si2323
$\text{O} + \text{TiH}^+ \rightarrow \text{TiO}^+ + \text{H}$	4.e-10	0	0	Si3977
$\text{O} + \text{TiH}_2^+ \rightarrow \text{TiOH}^+ + \text{H}$	6.3e-10	0	0	Si3978
$\text{O} + \text{TiC}^+ \rightarrow \text{TiO}^+, \text{C}$	6.e-10	0	0	Si3974
$\text{O} + \text{TiO}^+ \rightarrow \text{O}_2 + \text{Ti}^+$	2.e-10	0	0	Si3985
$\text{O} + \text{TiNC}^+ \rightarrow \text{TiN}^+ + \text{CO}$	1.e-10	0	0	Si3983
$\text{OH} + \text{Ti}^+ \rightarrow \text{TiO}^+ + \text{H}$	6.3e-10	-0.5	0	Si4030
$\text{OH}^+ + \text{Ti} \rightarrow \text{TiH}^+ + \text{O}$	1.9e-9	0	0	Si4012
$\text{OH}^+ + \text{TiH} \rightarrow \text{TiH}_2^+ + \text{O}$	1.e-9	0	0	Si4014
$\text{OH}^+ + \text{TiC} \rightarrow \text{HCTi}^+ + \text{O}$	4.5e-9	-0.5	0	Si4013
$\text{OH}^+ + \text{TiO} \rightarrow \text{TiOH}^+ + \text{O}$	9.e-10	-0.5	0	Si4015

Continuation of Table 1				
Reactions	α	β	γ	Ref
$\text{NH}_3 + \text{TiH}^+ \rightarrow \text{Ti} + \text{NH}_4^+$	1.e-9	-0.5	0	Si3824
$\text{NH}_3 + \text{TiOH}^+ \rightarrow \text{NH}_4^+ + \text{TiO}$	2.5e-9	-0.5	0	Si3825
$\text{NH}_3 + \text{HTiS}^+ \rightarrow \text{NH}_4^+ + \text{TiS}$	9.7e-10	-0.5	0	Si3812
$\text{H}_2\text{O} + \text{Ti}^+ \rightarrow \text{TiOH}^+ + \text{H}$	2.30e-10	-0.5	0	Si2790
$\text{H}_2\text{O} + \text{TiH}^+ \rightarrow \text{Ti} + \text{H}_3\text{O}^+$	8.e-10	-0.5	0	Si2792
$\text{H}_2\text{O} + \text{HNTi}^+ \rightarrow \text{TiN} + \text{H}_3\text{O}^+$	2.e-9	-0.5	0	Si2772
$\text{H}_2\text{O} + \text{HTiS}^+ \rightarrow \text{TiOH}^+ + \text{H}_2\text{S}$	1.1e-9	-0.5	0	Si2777
$\text{H}_3\text{O}^+ + \text{Ti} \rightarrow \text{TiH}^+ + \text{H}_2\text{O}$	1.8e-9	0	0	Si3039
$\text{H}_3\text{O}^+ + \text{TiH} \rightarrow \text{TiH}_2^+ + \text{H}_2\text{O}$	9.7e-10	0	0	Si3045
$\text{H}_3\text{O}^+ + \text{TiC} \rightarrow \text{HCTi}^+ + \text{H}_2\text{O}$	3.e-9	-0.5	0	Si3042
$\text{H}_3\text{O}^+ + \text{TiO} \rightarrow \text{TiOH}^+ + \text{H}_2\text{O}$	2.0e-9	-0.5	0	Si3047
$\text{HF} + \text{Ti}^+ \rightarrow \text{TiF}^+ + \text{H}$	5.7e-9	-0.5	0	Si3236
$\text{C}_2 + \text{TiO}^+ \rightarrow \text{TiC}^+ + \text{CO}$	7.6e-10	0	0	Si1686
$\text{C}_2\text{H} + \text{Ti}^+ \rightarrow \text{TiC}_2^+ + \text{H}$	1.e-9	0	0	Si1972
$\text{C}_2\text{H}_2^+ + \text{Ti} \rightarrow \text{TiC}_2^+ + \text{H}_2$	2.e-10	0	0	Si1750
$\text{HCN} + \text{Ti}^+ \rightarrow \text{TiNC}^+ + \text{H}$	1.4e-12	-0.5	0	Si3106
$\text{HNC} + \text{Ti}^+ \rightarrow \text{TiNC}^+, \text{H}$	1.e-9	-0.5	0	Si3267
$\text{HCN} + \text{HTiS}^+ \rightarrow \text{HCNH}^+ + \text{TiS}$	6.1e-10	-0.5	0	Si3101
$\text{CO} + \text{HNTi}^+ \rightarrow \text{TiN} + \text{HCO}^+$	2.e-9	0	0	Si2508
$\text{CO} + \text{TiO}^+ \rightarrow \text{CO}_2 + \text{Ti}^+$	7.9e-10	0	0	Si2513
$\text{HCNH}^+ + \text{Ti} \rightarrow \text{TiNC}^+ + \text{H}_2$	5.e-10	0	0	Si3117
$\text{H}_2\text{NC}^+ + \text{Ti} \rightarrow \text{TiNC}^+ + \text{H}_2$	5.e-10	0	0	Si2723
$\text{Ti} + \text{HCO}^+ \rightarrow \text{TiH}^+ + \text{CO}$	3.3e-10	0	0	S3210
$\text{Ti}^+ + \text{C}_2\text{H}_5\text{OH} \rightarrow \text{TiOH}^+ + \text{C}_2\text{H}_5$	2.2e-9	-0.5	0	Si4080
$\text{Ti}^+ + \text{HC}_4\text{H} \rightarrow \text{C}_4\text{H}^+ + \text{TiH}$	1.6e-9	0	0	SiRATE12
$\text{Ti}^+ + \text{NCCN} \rightarrow \text{TiNC}^+ + \text{CN}$	1.5e-10	0	0	Si4091
$\text{Ti}^+ + \text{OCS} \rightarrow \text{TiS}^+ + \text{CO}$	9.e-10	0	0	Si409
$\text{HCO}^+ + \text{TiH} \rightarrow \text{TiH}_2^+ + \text{CO}$	8.7e-10	0	0	Si3223
$\text{HCO}^+ + \text{TiC} \rightarrow \text{HCTi}^+ + \text{CO}$	2.e-9	-0.5	0	Si3218
$\text{HCO}^+ + \text{TiO} \rightarrow \text{TiOH}^+ + \text{CO}$	7.9e-10	-0.5	0	Si3226
$\text{HCO}^+ + \text{TiS} \rightarrow \text{HTiS}^+ + \text{CO}$	3.3e-9	-0.5	0	Si3227
$\text{TiH} + \text{S}^+ \rightarrow \text{TiS}^+ + \text{H}$	4.2e-10	0	0	Si4106
$\text{TiH}_2^+ + \text{O}_2 \rightarrow \text{TiOH}^+ + \text{OH}$	2.4e-11	0	0	Si4103
$\text{TiH}_2^+ + \text{S} \rightarrow \text{HTiS}^+ + \text{H}$	1.1e-9	0	0	Si4104
$\text{O}_2 + \text{TiS}^+ \rightarrow \text{SO}^+ + \text{TiO}$	6.23e-11	0	0	Si3896
$\text{O}_2 + \text{TiS}^+ \rightarrow \text{TiO}^+ + \text{SO}$	2.67e-11	0	0	Si3897
$\text{S} + \text{TiO}^+ \rightarrow \text{SO} + \text{Ti}^+$	1.e-9	0	0	Si4063
$\text{H}_2\text{S} + \text{HTiS}^+ \rightarrow \text{H}_3\text{S}^+ + \text{TiS}$	2.9e-10	-0.5	0	Si2801
$\text{H}^+ + \text{Ti} \rightarrow \text{Ti}^+ + \text{H}$	9.9e-10	0	0	Si418
$\text{H}^+ + \text{TiH} \rightarrow \text{TiH}^+ + \text{H}$	1.7e-9	0	0	Si431
$\text{H}^+ + \text{TiH}_2 \rightarrow \text{TiH}_2^+ + \text{H}$	1.5e-9	0	0	Si428
$\text{H}^+ + \text{TiC} \rightarrow \text{TiC}^+ + \text{H}$	3.e-9	-0.5	0	Si425
$\text{H}^+ + \text{HCTi} \rightarrow \text{HCTi}^+ + \text{H}$	1.5e-9	0	0	Si392
$\text{H}^+ + \text{TiN} \rightarrow \text{TiN}^+ + \text{H}$	3.e-9	-0.5	0	Si432

Continuation of Table 1				
Reactions	α	β	γ	Ref
$H^+ + HNTi \rightarrow HNTi^+ + H$	1.5e-9	0	0	Si394
$H^+ + TiO \rightarrow TiO^+ + H$	1.e-9	0	0	1
$H^+ + TiC_2 \rightarrow TiC_2^+ + H$	3.e-9	-0.5	0	Si419
$H^+ + TiNC \rightarrow TiNC^+ + H$	3.e-9	-0.5	0	Si433
$H^+ + TiS \rightarrow TiS^+ + H$	1.50e-9	-0.5	0	Si435
$He^+ + Ti \rightarrow Ti^+ + He$	3.3e-9	0	0	Si528
$C^+ + Ti \rightarrow Ti^+ + C$	2.1e-9	0	0	Si194
$C^+ + TiH_2 \rightarrow TiH_2^+ + C$	1.e-9	0	0	Si201
$C^+ + TiC \rightarrow TiC^+ + C$	2.50e-9	-0.5	0	Si198
$C^+ + TiN \rightarrow TiN^+ + C$	1.e-9	-0.5	0	Si203
$C^+ + TiC_2 \rightarrow TiC_2^+ + C$	2.e-9	-0.5	0	Si195
$C^+ + TiS \rightarrow TiS^+ + C$	2.3e-9	-0.5	0	Si204
$CH^+ + Ti \rightarrow Ti^+ + CH$	2.e-10	0	0	Si257
$NH_3^+ + Ti \rightarrow Ti^+ + NH_3$	1.9e-9	0	0	Si597
$H_2O^+ + Ti \rightarrow Ti^+ + H_2O$	3.e-9	0	0	Si477
$Na + Ti^+ \rightarrow Ti + Na^+$	2.7e-9	0	0	Si645
$Mg + TiO^+ \rightarrow TiO + Mg^+$	1.e-9	0	0	Si541
$Ti + NO^+ \rightarrow NO + Ti^+$	1.6e-9	0	0	Si720
$Ti + P^+ \rightarrow P + Ti^+$	1.e-9	0	0	Si722
$Ti + O_2^+ \rightarrow O_2 + Ti^+$	1.6e-9	0	0	Si721
$Ti + S^+ \rightarrow S + Ti^+$	1.6e-9	0	0	Si723
$Ti + HS^+ \rightarrow HS + Ti^+$	1.4e-9	0	0	Si719
$Ti + H_2S^+ \rightarrow H_2S + Ti^+$	1.60e-9	0	0	Si718
$Ti + CS^+ \rightarrow CS + Ti^+$	1.50e-10	0	0	Si716
$HCO + TiO^+ \rightarrow TiO + HCO^+$	6.6e-10	-0.5	0	Si504
$TiH + S^+ \rightarrow S + TiH^+$	4.2e-10	0	0	Si724
$NO + TiO^+ \rightarrow TiO + NO^+$	7.2e-10	0	0	Si631
$S^+ + TiC \rightarrow TiC^+ + S$	3.7e-9	-0.5	0	Si705
$S^+ + TiS \rightarrow TiS^+ + S$	3.2e-9	-0.5	0	Si706
$TiO^+ + Fe \rightarrow Fe^+ + TiO$	1.e-9	0	0	Si725
$C^- + Ti^+ \rightarrow Ti + C$	7.51e-8	-0.5	0	Si4138
$Ti^+ + S^- \rightarrow S + Ti$	7.51e-8	-0.5	0	Si5084
$TiH^+ + e^- \rightarrow Ti + H$	2.e-7	-0.5	0	Si1498
$TiH_2^+ + e^- \rightarrow Ti + H + H$	2.e-7	-0.5	0	Si1500
$TiH_2^+ + e^- \rightarrow Ti + H_2$	1.5e-7	-0.5	0	Si1499
$TiH_2^+ + e^- \rightarrow TiH + H$	1.5e-7	-0.5	0	Si1501
$TiC^+ + e^- \rightarrow Ti + C$	2.e-7	-0.5	0	Si1471
$HCTi^+ + e^- \rightarrow Ti + CH$	1.5e-7	-0.5	0	Si1362
$HCTi^+ + e^- \rightarrow TiC + H$	1.5e-7	-0.5	0	Si1363
$TiN^+ + e^- \rightarrow Ti + N$	2.0e-7	-0.5	0	Si1508
$HNTi^+ + e^- \rightarrow Ti + NH$	1.5e-7	-0.5	0	Si1376
$HNTi^+ + e^- \rightarrow TiN + H$	1.5e-7	-0.5	0	Si1377
$TiO^+ + e^- \rightarrow Ti + O$	1.e-7	0	0	1
$TiOH^+ + e^- \rightarrow Ti + OH$	1.5e-7	-0.5	0	Si1515

Continuation of Table 1

Reactions	α	β	γ	Ref
TiOH ⁺ + e ⁻ → TiO + H	1.5e-7	-0.5	0	Si1516
TiF ⁺ + e ⁻ → Ti + F	2.0e-7	-0.5	0	Si1497
TiC ₂ ⁺ + e ⁻ → Ti + C ₂	1.5e-7	-0.5	0	Si1472
TiC ₂ ⁺ + e ⁻ → TiC + C	1.5e-7	-0.5	0	Si1473
TiNC ⁺ + e ⁻ → Ti + CN	3.0e-7	-0.5	0	Si1509
TiS ⁺ + e ⁻ → S + Ti	2.0e-7	-0.5	0	Si1517
HTiS ⁺ + e ⁻ → HS + Ti	1.5e-7	-0.5	0	Si1400
HTiS ⁺ + e ⁻ → TiS + H	1.5e-7	-0.5	0	Si1401
Ti ⁺ + e ⁻ → Ti + PHOTON	4.26e-12	-0.62	0	Si6178
H + Ti ⁺ → TiH ⁺ + PHOTON	1.17e-17	-0.14	0	Si6127
H ₂ + Ti ⁺ → TiH ₂ ⁺ + PHOTON	3.e-18	0	0	Si6114
O + Ti ⁺ → TiO ⁺ + PHOTON	9.22e-19	-0.08	-21.2	Si6136
O + Ti → TiO + PHOTON	5.52e-18	0.31		Si6137
Ti + PHOTON → Ti ⁺ + e ⁻	3.1e-9	0	2.3	Si6017
TiH + PHOTON → Ti + H	2.8e-9	0	1.6	Si6038
TiH ⁺ + PHOTON → Ti ⁺ + H	2.7e-9	0	1.2	Si6029
TiC + PHOTON → Ti + C	1.0e-10	0	2.3	Si6025
TiO + PHOTON → Ti + O	1.6e-9	0	2.3	Si6044
TiO + PHOTON → TiO ⁺ + e ⁻	2.4e-10	0	2	Si6045
TiO ⁺ + PHOTON → Ti ⁺ + O	1.0e-10	0	2	Si6042
TiS + PHOTON → S + Ti	1.0e-10	0	2.3	Si6046
Ti + CRPHOT → Ti ⁺ + e ⁻	2115	0	0	Si4424
TiH + CRPHOT → Ti + H	250	0	0	Si980
TiC + CRPHOT → Ti + C	250	0	0	Si974
TiO + CRPHOT → Ti + O	250	0	0	Si984
TiS + CRPHOT → S + Ti	250	0	0	Si985
Ti + O → TiO ⁺ + e ⁻	1.0e-11	0	1973	chu80,opp77
TiO ⁺ + e ⁻ → TiO + PHOTON	5.0e-10	0	0	chu80
Ti ⁺ + O ₂ → TiO ⁺ + O	1.0e-9	0	0	1
Ti ⁺ + H ₂ O → TiO ⁺ + H ₂	1.0e-9	0	0	1
TiO ⁺ + Ca → TiO + Ca ⁺	1.0e-9	0	0	chu80
TiO ⁺ + Na → TiO + Na ⁺	1.0e-9	0	0	chu80
TiO ⁺ + Al → TiO + Al ⁺	1.0e-9	0	0	chu80
TiO ⁺ + K → TiO + K ⁺	1.0e-9	0	0	chu80
TiO + C → Ti + CO	1.0e-10	0	0	chu80
Ti ⁺ + CH ₃ OH → TiOH ⁺ + CH ₃	1.65e-9	-0.5	0	Si4088
TiH + H → Ti + H ₂	8.3e-11	0	0	2
TiH + O → Ti + OH	1.66e-10	0	0	2
TiH + CH ₃ → Ti + CH ₄	1.0e-10	0	0	2
TiC + H → Ti + CH	1.0e-10	0	20109	2
Ti + CO → TiC + O	8.0e-10	0	68842	2
Ti + CN → TiC + N	5.0e-10	0	29543	2
Ti + NO → TiN + O	5.0e-11	0	19706.	2
TiN + H → Ti + NH	1.e-10	0	15655	2

Continuation of Table 1				
Reactions	α	β	γ	Ref
Ti + NO → TiO + N	9.e-11	-0.96	0	2
TiO ₂ + O → TiO + O ₂	1.e-10	0	11877	2
TiO ₂ + CO → TiO + CO ₂	1.e-10	0	9160	2
TiO + O → Ti + O ₂	5.42e-13	0	20794	2
TiO + N → Ti + NO	4.76e-12	0	4772	2
TiO + N ₂ → Ti + N ₂ O	5.9e-12	0	62193	2
Ti + CO ₂ → TiO + CO	7.01e-11	0	1790	2
TiO + NO → TiO ₂ + N	7.8e-12	0	0	3
TiO + O ₂ → TiO ₂ + O	1.5e-12	0	0	3
TiO + N ₂ O → TiO ₂ + N ₂	4.e-13	0	0	3
End of Table				